Contaminant Cation Effect on Oxygen Transport Through the Ionomers of Polymer Electrolyte Membrane Fuel Cells

Jonathan P. Braaten[a], Xiaomin Xu[a], Yun Cai[b], Anusorn Kongkanand[b], and Shawn Litster[a,*]

[a]Mechanical Engineering Department, Carnegie Mellon University, Pittsburgh, PA, USA

[b]General Motors Fuel Cell Activities, Pontiac, MI, USA

*Corresponding Author (litster@andrew.cmu.edu)

Abstract

In this work, we characterized the effects of cobalt (Co) and other cation contaminants on the oxygen transport properties of the perfluorosulfonic acid (PFSA) ionomer used in polymer electrolyte membrane fuel cells and gained insight into the mechanisms by which contaminant cations inhibit oxygen (O_2) transport. Such cations can be released by alloy catalysts and pose a significant challenge to maintaining high current density performance with low platinum (Pt) loading. To measure the cation effect on O_2 transport, we used a test cell capable of isolating the ionomer from the membrane electrode assembly (MEA), allowing for oxygen transport resistance (R_{O2}) measurements using a limiting current technique. We contaminated ionomer membranes with Co at various loadings and found a general increase in R_{O2} for increased cation contamination levels and decreased water activity. In addition, our results indicated distinct cation concentration dependent regimes, where low contamination levels caused little to no increase in the R_{O2}, and high contamination levels caused a significant increase in the R_{O2}. We also performed experiments on ionomer membranes fully contaminated with lithium (Li), sodium (Na), nickel (Ni), and cerium (Ce) to evaluate the effect of valency, ion pairing strength, and membrane hydration. The results for the divalent cations (Ni and Co) were nearly identical, but the results for the monovalent cations differed significantly, with Li cations having less of an effect on oxygen transport than Na. A minimal loading of Ce (~5%) was also studied and had a negligible impact on oxygen transport. These experiments showed that the origins of the increased R_{O2} with cation poisoning are stronger ion pairing, reduced water uptake, and cross-linking for the multivalent cations in PFSA films. We believe that each of these mechanisms result in a more compressed and tortuous hydrophilic domain and oxygen diffusion path, and a

commensurate increase in R_{O2}. We found that an increased water content can help reduce these impacts through electrostatic shielding between the cations and sulfonate groups.

Introduction

Polymer electrolyte membrane fuel cells (PEMFCs) are a promising technology to deliver clean, sustainable power, especially for transportation applications. Their high efficiency, scalable power, and energy density demonstrate their promise as a clean energy conversion technology for long-range and heavy-duty transportation applications such as commercial trucks, public transit buses, standard duty pickups, and long-range family vehicles. However, this technology is currently not cost competitive with the incumbent internal combustion (IC) engine. Reduction in usage amount of Pt is imperative in order to reduce cost and to not disrupt the demand-supply balance of the precious metal market when fuel cell vehicle volume increases. (1, 2).

As the Pt catalyst loading is reduced in the cathodes of PEMFCs, the total number of accessible catalytic sites is reduced, and the oxygen flux through the thin films of ionomer in the catalyst layers becomes higher and more concentrated. This has resulted in a mass transport limited current caused by high local oxygen transport resistances (R_{O2}^{Pt}), as illustrated by previous works (2, 3). These high R_{O2}^{Pt}'s result in lower current densities and lower power output, preventing PEMFC developers from further reduce the Pt amount. Compounding this already substantial performance reduction, contaminant cations have been shown to decrease the limiting current density of PEMFCs, which is thought to be partially the result of an increase in the local resistance (4-8). These contaminant cations can be introduced to the ionomer by unstable alloy catalysts like PtNi or PtCo (4, 9), environmental sources such as road salts (NaCl, $CaCl_2$, etc.) or water contaminants, or from cation sources intentionally added to PEMFCs, such as the cerium (Ce) used as a radical scavenger inside the membranes of PEMFCs (10). These contaminant cations have been shown to preferentially exchange with the protons in the ionomer, preventing the ionomer's sulfonate groups from conducting protons and inhibiting oxygen transport within the cathode catalyst layers (CCLs) (4, 6, 8). While significant efforts have been made to understand the role of these contaminant cations in reducing proton conductivity, little has been done to quantify or understand their effects on the oxygen transport through the ionomer in CCLs.

Some literature (4, 6-8, 16) have also reported the effects of similar cations on the water content and structure of contaminated ionomers. Their results have indicated reduced water uptake for contaminant cation-form membranes, with lesser uptake witnessed for larger radius cations (16). This water loss is significant, due to the well-established conclusion that the oxygen permeability of ionomer membranes is highly dependent on the water content (17-19). Thus, any reduction in the ionomer's water content would cause fuel cell performance losses due to lower oxygen permeability of the membranes of the CCLs.

Another relevant hypothesis was made by Shi et al. (16) based on their observed increase in modulus (stiffness) for contaminant cation-form ionomers. Their results indicated the establishment of cross-links between sulfonate groups within the hydrophilic domains of the ionomer for higher valency cation-form membranes as well as stronger ion pairing between the cations and the sulfonate groups (16). This enhanced cross-linking and ion pairing is thought to be significant, due to the suspected increase in hydrophilic domain tortuosity, which would result in longer diffusion lengths in addition to the reduced water contents of the ionomer.

The purpose of this work is to quantify the effects of cation contamination of the ionomer used in CCLs, in terms of their R_{O2}. Cobalt (Co) was selected as the primary cation contaminant in this study, due to its demonstrated ability to boost the catalytic performance when alloyed with Pt (9, 11). While these PtCo alloys meet the 2020 DOE targets for performance in terms of beginning of life mass activity and total platinum group metal loading (2), extensive testing has indicated significant performance losses for cycled stacks due to the presence of leached Co in the ionomer (4, 5)(12, 13)

We also performed experiments with several other cations frequently encountered in PEMFCs. Nickel (Ni) was chosen, for the same reason as Co; it is used as an alloying element to boost catalytic activity (11). Ce was chosen, due to its use as a radical scavenger in the membrane and demonstrated (negative) effect on oxygen transport in PEMFC CCLs (14, 15). The remainder of the cations tested (Li, Na) were studied to determine the effects of monovalent cations, as opposed to divalent cations like Co and Ni, and trivalent Ce. These cations gave us an adequate study group to develop hypotheses on the effects of valency, ion pairing, hydration state, and contamination level.

In an earlier study, we have successfully developed an apparatus capable of measuring O2 transport resistance as a function of ionomer membrane thickness (3). We found that the resistance was linearly proportional to the membrane thickness in the range of 50 to 2000 nm. In this study, we use this apparatus to study the O2 resistance as a function of cation content and species. We discuss how RO2 changes with cation poisoning through stronger ion pairing, cross-linking, and reduced water uptake. We then discuss how these results can be applied to the effects observed in a fuel cell.

Experimental Method

In order to measure the distinct effect of contaminant cations on oxygen transport through the PFSA ionomer, we had to isolate the oxygen transport losses from the proton conduction losses and cation accumulation, which is difficult to accomplish when analyzing contaminated MEAs. In addition, we needed to eliminate the confinement and interfacial effects found in CCLs' ionomer films (20, 21) and the gradients in contaminant cation concentration in polarized MEAs (4, 12, 13). Therefore, we designed a test cell utilizing an unsupported (no interfacial or confinement effects) and non-polarized (no proton conduction current or contaminant concentration gradient) ionomer membrane. The samples were prepared as described in the following section and were then tested as described in the *Experimental Setup* and *Testing Procedure* sections.

Ionomer Contamination Procedure

We prepared ionomer membrane samples (Nafion N117, Ion Power, New Castle, DE) contaminated with Li, Na, Ni, Co, and Ce cations using a method similar to that of Greszler et al. (4). The samples were cut from an as-received sheet of Nafion N117 PFSA membrane and purified by boiling for one hour in a 3% hydrogen peroxide (Certified, Fisher Scientific, Waltham, MA) solution to remove contaminants and impurities. Next, they were soaked for another hour in near-boiling de-ionized (DI) water to remove the hydrogen peroxide and then boiled for one hour in 0.5 M sulphuric acid (Reagent Grade, Sigma Aldrich, St. Louis, MO) to re-protonate the samples. Lastly, they were soaked for one hour in near-boiling DI water and then stored in DI water.

Intermediate Cobalt Contamination Process

The purified membrane samples were contaminated in batches of 4 pieces using aqueous solutions of cobalt nitrate (Reagent Grade, Sigma Aldrich, St. Louis, MO) and nitric acid (Reagent Grade, Sigma Aldrich, St. Louis, MO) to vary the Co and proton concentrations. We soaked the membrane samples for at least two days, replacing the solution after the first day to ensure the exchange solution would not be cation depleted to the point where the exchange would be incomplete. The samples were then rinsed in DI water and dried prior to being humidified and analyzed in the R_{O2} test cell. The levels of Co contamination were measured using inductively coupled plasma optical emission spectroscopy (ICP-OES) (RJ Lee Analytical Chemistry Group, Pittsburgh, PA) and the resulting Co exchange isotherm is presented in Figure 1. Note that the proton fraction, ξ, has been defined by Greszler et al. (4) as:

$$\xi = \frac{c_{\mathrm{H}^+}}{2(c_{\mathrm{Co}^{2+}}) + c_{\mathrm{H}^+}} \tag{1}$$

where c_{H^+} is the concentration of protons in the sample and $c_{\mathrm{Co}^{2+}}$ is the concentration of Co cations in the sample.

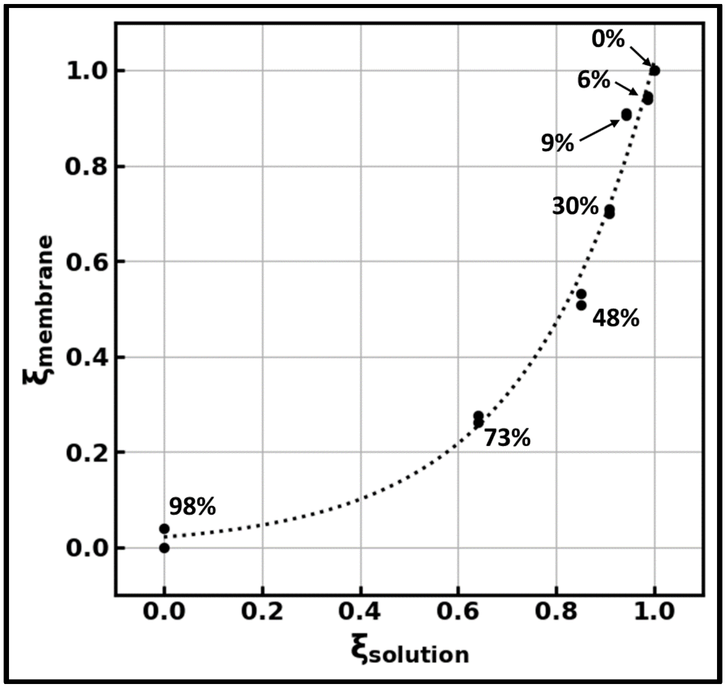

Figure 1. Co exchange relation from solution to membrane, where ξ is the proton fraction from Eq. 1. Note that the percentages shown are the average Co levels of 2 samples.

Cation Comparison Study Contamination Process

We prepared aqueous solutions of lithium sulfate, sodium sulfate, nickel sulfate, cobalt sulfate, and cerium sulfate (Reagent Grade, Sigma Aldrich, St. Louis, MO) for the cation comparison experiments, similar to the Co exchange process but without the nitric acid. For all cation types except Ce, we accomplished full exchanges, again verified by ICP-OES. For the Ce samples, we accomplished only a 5% exchange, due to the limited solubility of cerium sulfate, which prevented the Ce cations from being absorbed by the membrane samples.

<u>Experimental Setup</u>

To create an R_{O2} measurement cell, we modified existing commercial fuel cell hardware (Dual Area Fuel Cell Fixture, Scribner and Associates, Southern Pines, NC), similar to that of our prior work in Liu et al. (3). The cell consisted of a modified cathode flow plate and sample holder with a free-standing, electrically isolated membrane sample, and a fuel cell MEA (4 cm^2 active area) functioning as an oxygen sink and oxygen transport rate monitor. The anode side of the Scribner cell remained unchanged. The R_{O2} test cell's design is shown in Figure 2. This setup allowed for the bulk measurement of the R_{O2} of cation contaminated membrane samples, while eliminating the confinement, interfacial, conductivity, and electrical gradient effects found in operating MEAs. Thus, the measurements from this setup provided the pure, bulk R_{O2} effects of cation contaminants and allowed valuable insight into the mechanisms of the observed decrease in oxygen transport for cation contaminated MEAs.

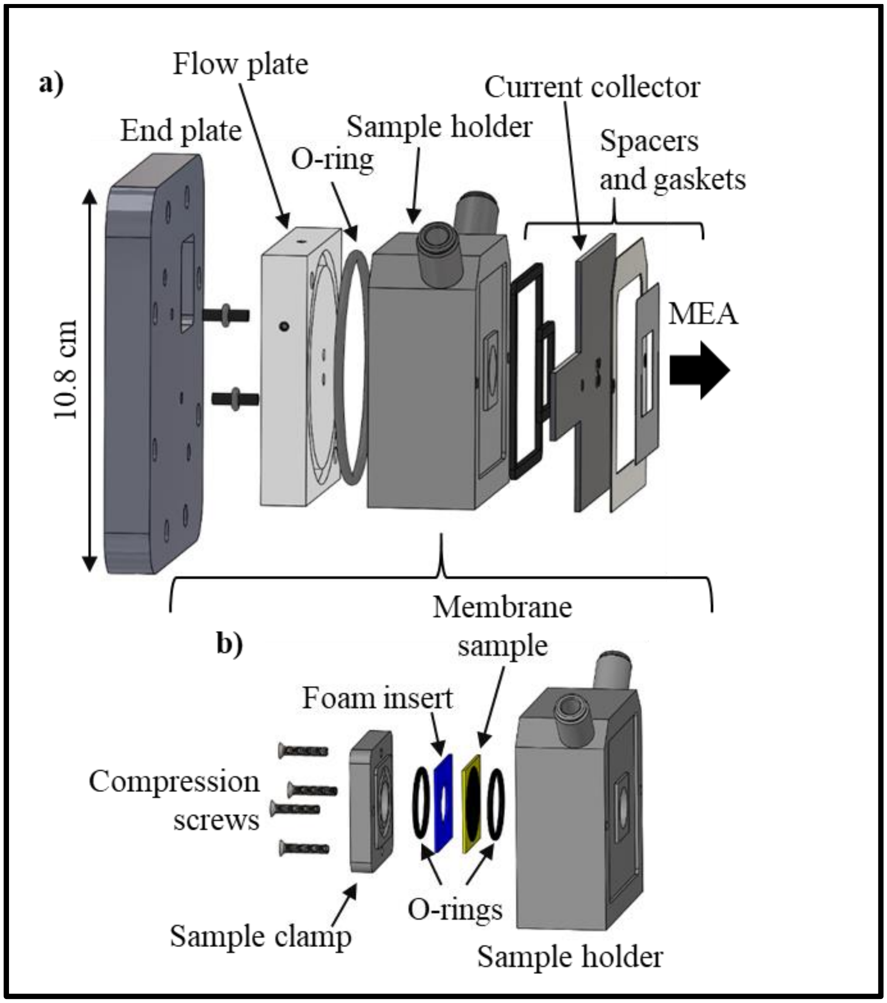

Figure 2. a) Exploded view of the cathode side of the test cell assembly. The anode side of the assembly remained unchanged from the fuel cell hardware. b) Exploded view of the sample holder assembly. Note that the foam insert was used to prevent condensation buildup on the sample during testing. The diameter of the sample's test area is 14 mm.

Once the contaminated membrane sample was installed, we supplied air to the top of the membrane sample and operated the test cell's MEA under its limiting current regime (0.4 and

0.3V). This allowed us to drive the oxygen concentration to roughly zero below the sample as shown in Figure 3, enabling the application of a Faradaic Ohm's Law analogy for the R_{O2}:(3)

$$R_{\mathrm{O}_2} = \frac{nAFc_{\mathrm{O}_2,a}}{I} \tag{2}$$

where n is the number of electrons transferred per mole of fuel (4 for oxygen, in this case), A is the area of the membrane sample, F is Faraday's constant, $c_{\mathrm{O}_2,a}$ is the oxygen concentration above the sample from the feed gas, and I is the current produced by the MEA, which served as the oxygen sink.

While this approach to measuring the R_{O2} includes both the non-equilibrium absorption resistance at the gas/membrane interface ($R_{\mathrm{O}_2}^{abs}$ in Figure 3) as well as the non-equilibrium desorption resistance at the membrane/gas interface ($R_{\mathrm{O}_2}^{des}$ in Figure 3), these resistances have been shown to be negligible compared to the diffusive resistance through the membrane, especially for bulk ionomer membranes (3). Also, the R_{O2} due to diffusion through the oxygen depleted zone from the bottom of the sample to the CCL of the test cell's MEA has been calculated to be several orders of magnitude smaller than the resistance due to diffusion through the uncontaminated membrane sample. Thus, the total resistance ($R_{\mathrm{O}_2}^{tot}$ in Figure 3) measured by our method is dominated by the $R_{\mathrm{O}2}$ due to diffusion through the membrane sample ($R_{\mathrm{O}_2}^{diff}$ in Figure 3).

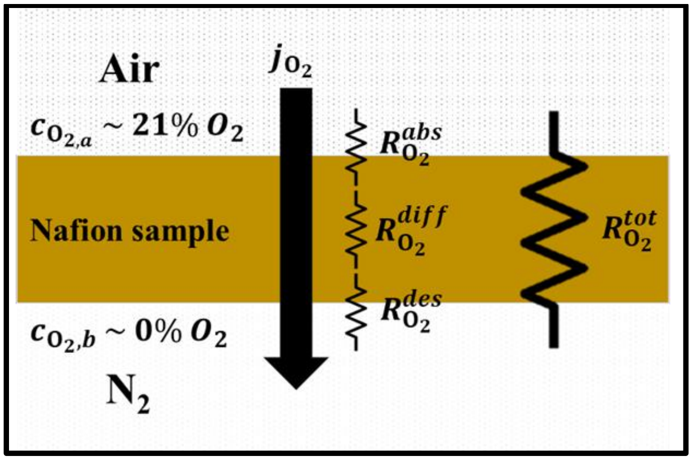

Figure 3. R_{O2} resistance network from the cathode stream to the oxygen depleted zone below the membrane sample. Note the known concentrations of oxygen above and below the sample, which are used in Eq. 2.

<u>Testing Procedure</u>

We tested the samples by clamping them in the sample holder assembly as shown in Figure 2b, and then assembling the remainder of the test cell shown in Figure 2a. The cell was heated to 80°C at 1 atm, and the relative humidity (RH) of the cathode and anode streams were controlled using the humidifier temperature. Two different experimental procedures were used: one for the intermediate Co loading experiment and one for the cation comparison experiment. For the intermediate Co loading experiments, the anode's RH was held at 40%, and the cathode's RH was varied from 40% to 80% to reflect low (40%), medium (60%) and high (80%) water contents in the contaminated membrane samples. For the cation comparison experiments, the relative humidities of the anode and cathode were varied together between 40% and 100% RH to test the effects of low, medium, high, and fully humidified membrane samples.

We performed the experiments by holding the test cell's MEA at 0.4 and 0.3 V, which were established as the limiting current voltages in preliminary experiments. A background current was established using nitrogen (N_2) on the cathode, and pure hydrogen (H_2) on the anode. Once the background current stabilized, we switched the N_2 supply to air (21% O_2) and again held the test cell at 0.4 and 0.3 V until the current stabilized for each voltage. This allowed for the current due to oxygen permeation through the membrane sample to be determined by evaluating the difference between the N_2/H_2 background and air/H_2 currents. We used the current from the 0.3 V holds to calculate the R_{O2} as described in Eq. 2. During measurements, we would occasionally observe irregular disturbances, especially at low MEA RH, which we attributed to MEA instability in our test cell. These sections of data were omitted from the subsequent current averaging methods used to find the background and oxygen permeation currents. Figure 4 shows an example of the raw current data from the testing procedure, along with the difference in currents used for the resistance calculation.

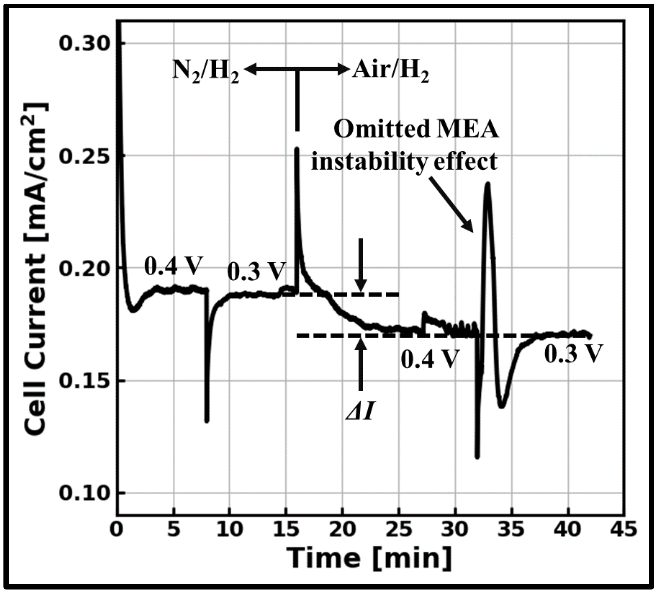

Figure 4. Raw current data from the experimental procedure. The current difference (*ΔI*) between the N_2/H_2 and air/H_2 environments at 0.3 V represents the current produced due to oxygen permeation through the ionomer.

<u>MEA O2 Limiting Current Testing</u>

The local oxygen transport resistance of the MEAs was obtained via the oxygen limiting current study (DOI: 10.1149/1.3152226 and 10.1149/2.061212jes). Specifically, 18-micron thick PFSA membranes with internal reinforced layer were doped with given levels of Co^{2+} following the procedure given above. MEAs with an active area of 5 cm^2 were prepared by hot pressing the cobalt-doped membrane with electrode decals at 295 ^{o}C, 5000 lb for two minutes. The cathodes were a 10 wt% Pt/Vulcan at a loading of 0.05 mg_{Pt}/cm^2. The cathode thickness was measured to be ~10 µm by Scanning Electron Microscopy. All anodes were 20 wt% Pt/GrC (graphitized carbon) at a loading of 0.05 mg_{Pt}/cm^2.

Low-pressure drop flowfields were used to enable operation at high flows (stoichiometry of >15) without significant down-channel pressure drop and thus the gas composition variation through the cell. The limiting current measurements were performed at 80 °C, 62% RH with three dry mole fractions of oxygen at 0.01, 0.02, and 0.04 at four different pressures, 110, 150, 200 and 300 kPa. The measurements were run at sub-saturated conditions such that liquid water effects could be neglected. Diluted oxygen concentrations were chosen to reduce the limiting current density and keep the product water in a vapor form, as well as simplification of the transport model by enabling the use of Fick's law. A minimum of three replicates were tested for each level of cation.

Results and Discussion

First, we present the results for the Co contaminated membranes with the contamination levels shown in Figure 1. We tested at least 3 membrane samples per contamination level, and the data for each water content (low, medium, high) was averaged once a steady state current reading was achieved. The data for each contamination level is shown in Figure 5. It is important to note that no error bars accompany Figure 5. This was done for the sake of clarity of the figure, and the raw data sets and the averages for each sample batch are provided for reference in the supplementary information, Figures SA1-7.

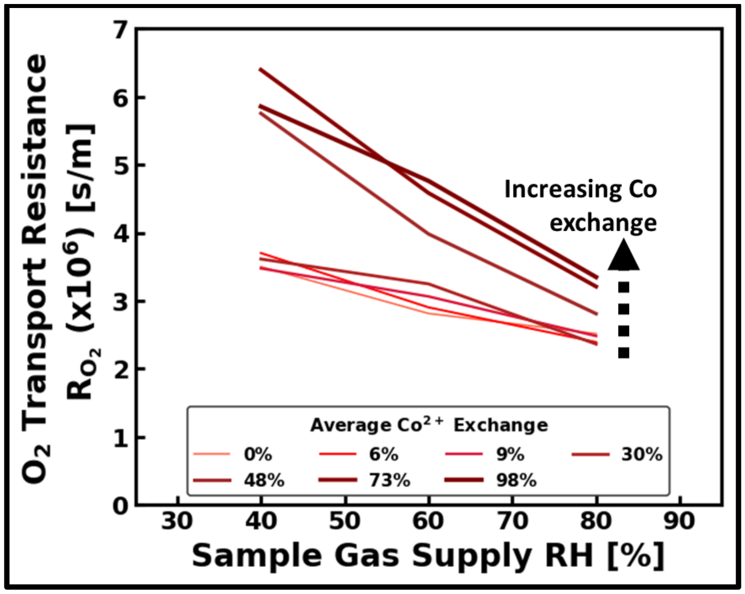

Figure 5. Averaged R_{O2} results for all Co contamination levels tested. Note that the Co exchange percentage reflects the percentage of sulfonate groups occupied by Co cations.

As shown in Figure 5, while R_{O2} increases with decreasing gas supply RH, the R_{O2} increase is significantly higher with increasing Co contents. This was supported by MEA testing results (5) that observed apparent increase in R_{O2} with Co cation contamination, especially, under dry operation. Previous studies [e.g. http://dx.doi.org/10.1016/j.electacta.2016.10.096] showed that the effect on the membrane water uptake due to the presence of cation is more obvious in the low water content (Lambda) regime where most of the water still bound to the ionomer acid sites and the sulfonate/cation interactions dominate.

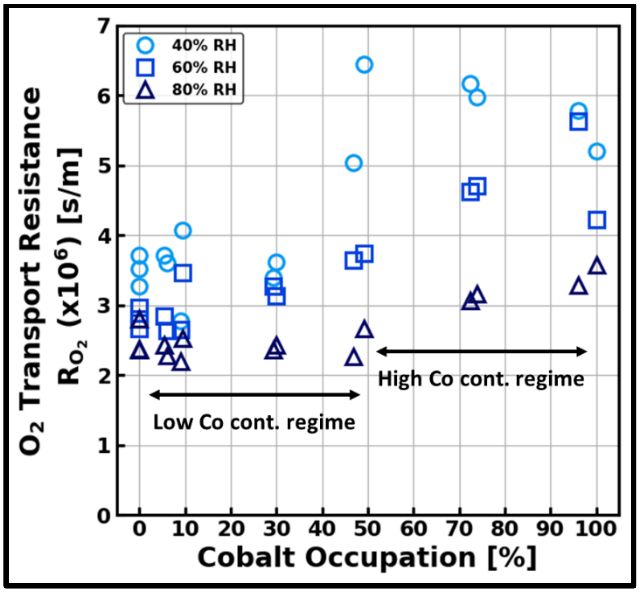

Figure 6. R_{O2} as function of sample Co content (non-averaged ICP-OES results) for each water content tested.

Further examination of the R_{O2} increases shows that there was little change in R_{O2} when the Co content was below 30% and that the high Co contamination (48% and above) results corresponded well with the fully contaminated results. This bimodal grouping of the R_{O2} results is further examined in Figure 6, where we present the R_{O2} as a function of the Co contamination level. Between the low and high contamination regimes (~50% exchange), a sharp increase in R_{O2} is present, which suggests a critical concentration where the Co cations begin to cause significant structural changes to the membranes' hydrophilic domains, causing an increase in the R_{O2}. The hydration state of the membranes may also play a role in suppressing these structural changes, as illustrated by the difference in the R_{O2} increase between the low and high contamination regimes for each hydration state.

To further explore and decouple the phenomena affecting the membrane samples' hydrophilic domains, we performed experiments with fully exchanged membranes using cations of varying radius and valency under varying hydration states (40-100% RH). The results from this study are shown in Figure 7. Again, the error bars were omitted for clarity, and the raw datasets for each cation type are shown in the supplementary materials, Figures SB1-6.

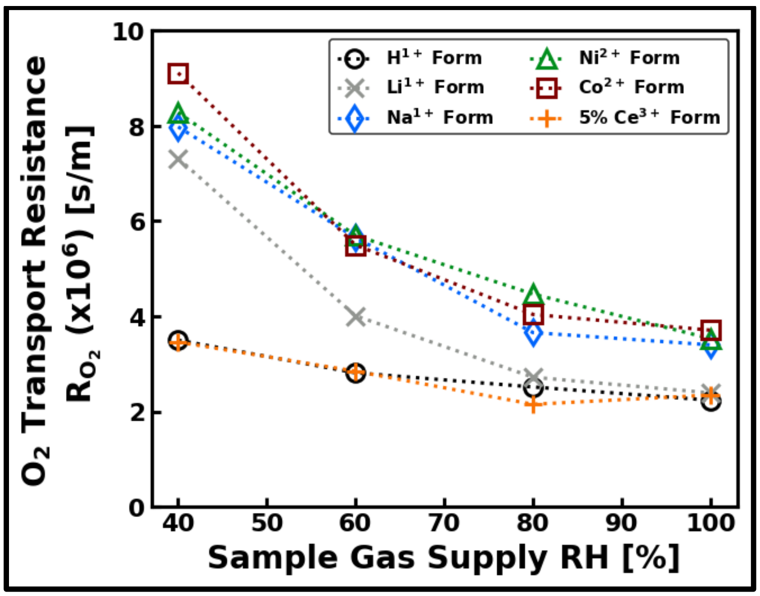

Figure 7. R_{O2} of various cation-form Nafion N117 membranes.

The data in Figure 7 shows several trends. First, the divalent and similarly sized Ni and Co cations had much the same effect on oxygen transport, as expected. However, the results for the monovalent Na and Li samples differ significantly between each other. The Na results were similar to the dual valency Co and Ni results, whereas the Li was more similar to the proton form membranes at high water activity (80 and 100% RH) and the Na, Co, and Ni results at low water activity (40% RH). However, it is important to note that due to the valency of Ni and Co, the concentration of these two cations is half that of Na and Li per electroneutrality in the samples.

The 5% Ce exchange had little to no impact on the R_{O2}, validating the uncontaminated (proton form) base case.

The experimental results illustrated in the previous paragraphs provided a basis from which we can compare the effects of each mechanism: ion pair strength, reduced water uptake, and ionic cross-linking. In the following paragraphs, we will use our experimental results to develop hypotheses on the structural changes of ionomer membranes contaminated with cations of various radius and valency and their effect on overall fuel cell performance. In addition, we will postulate on the contribution of each mechanism to the structural changes associated with the exchange of protons with contaminant cations in ionomer membranes.

Studying the results of the membranes in proton and Li form allows for the evaluation of the impact of ion pair strength. Using the proton form membrane as a baseline (Figure 7), the increase to the Li results are purely the result of stronger ion pairs. Li is known to not cause a reduction in water uptake to the membrane (16). In addition, it cannot cause cross-linking due to its monovalent ionized state. As a result, the difference in results between the proton and Li form membranes can be attributed to stronger ion pairs. This is further shown by the magnitude of this change at low and high water contents. At 40% RH, the R_{O2} increases by nearly two-fold, and at 100% RH, the R_{O2} is not impacted. Since ion pair strength is known to be a function of hydration state, this result is consistent with ion pair theory. At lower hydration states, we expect for the ion pairs to become stronger, leading to a stiffer membrane matrix which is consistent with the increase in modulus for Li form membranes shown by Shi and colleagues (16). We suspect that with this increase in rigidity, the hydrophilic domains of the membrane become more tortuous, leading to a longer diffusion length for oxygen and a higher R_{O2}.

The comparison between the Na and Li form membranes (Figure 7) allowed for the separation of the reduced water uptake effect. As before, the concentration of protons, Li, and Na are all the same in the membrane and no cross-linking is possible. The difference in R_{O2} results between the Li form membranes and the Na form membranes can then be attributed to the effects of a reduction in water uptake. Na has been shown to reduce water uptake, which is known to impair gas permeability (17, 18). This reduction in water content is suspected to impact the membranes in two ways: reducing the hydrophilic domain size and allowing the ion pairs to become stronger due to reduced shielding. The former shrinks O_2's primary pathway through the membrane, and the latter is anticipated to cause increased rigidity and tortuosity in the membrane, as discussed previously. Both factors are suspected to contribute to the large increase in the R_{O2} observed for the Na form membranes. To illustrate these phenomena, Figure 8 shows the suspected effects of membrane dehydration due to Na (or similar monovalent cation) and the hydrophilic domain tortuosity increase from stronger ion pairs.

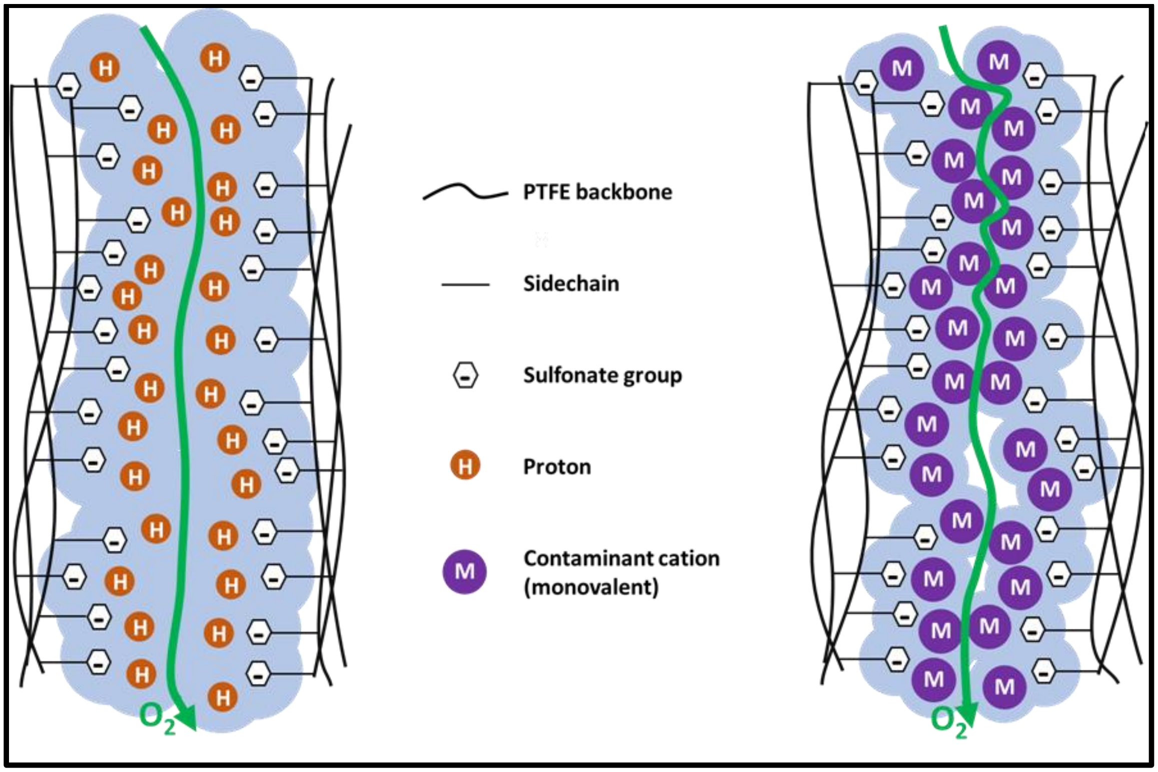

Figure 8. Hypothesized fully humidified proton-form ionomer (left) versus fully humidified monovalent contaminant cation-form ionomer (right). Note the distortion of the PTFE backbone of the contaminant cation-form ionomer due to the stronger ion pairs (i.e. the distance between the cations and the sulfonate groups).

The last mechanism, cross-linking, can be evaluated using the divalent Ni and Co datasets and comparing them to the monovalent Li and Na datasets (Figure 7). The water uptake loss for Na is greater than for most transition metals (16) like Co and Ni. In addition, the concentration of Ni and Co are half that of protons, Li, and Na, per electroneutrality. With Co and Ni having greater water uptakes (good for O_2 permeation) and weaker ion pair strengths due to the distance between sulfonate groups and greater hydration state, the cross-linking effect is thought to be the primary contributor to the increase in the R_{O2} seen in our Co and Ni datasets. Similar to the effect of stronger ion pairing, we suspect that the cross-linking of sulfonate groups with multivalent cations causes significant hydrophilic domain tortuosity, again causing reduced O_2 transport.

In contrast to the various cation experiments, the intermediate Co loading study sheds light on the impacts of incomplete exchanges. From the data we presented in Figures 5 and 6, we hypothesize that distinct contamination regimes exist above and below a contamination threshold, where the impact of the contaminant cations on the R_{O2} is large and small, respectively. For Co, we showed that this threshold is near 50% exchange. At this exchange level, we suspect that the hydrophilic domain structure begins to become more distorted, leading to longer diffusion paths for O_2 and a corresponding increase in the R_{O2}. In addition, we show that increased hydration states are able to suppress these effects by weakening the ion pair strengths and expanding the hydrophilic domains.

Last, we evaluate the R_{O2} of a fuel cell cathode using the limiting current test. [ref Baker/Grezsler/JPCL] The tests were done at different gas pressures to differentiate the pressure-dependent and pressure-independent components of the R_{O2}. As expected pressure-dependent R_{O2}, primarily from the gas diffusion media, were unaffected by the Co level. The pressure-independent resistances were then accounted for Knudsen diffusion in the microporous layer and electrode [ref Grezsler/JPCL], leaving only the O2 transport resistance that is local to Pt surface ($R_{O2,Pt}$). Figure 9 summarizes the measured $R_{O2,Pt}$ as a function of Co exchange level.

It is clear that increased Co levels results in increased $R_{O2,Pt}$, and that the resistance appears to reach a plateau. MEAs with higher Co levels were also tested, but unfortunately, high electrode proton resistance caused a non-linear limiting current vs O2 concentration correlation, hence, the data were removed. While it remains unclear the true origin of the $R_{O2,Pt}$, the resistance has been shown to be strongly related to how ionomer interacts with Pt surface [ref]. Therefore, it is understandable for cation to affect $R_{O2,Pt}$.

Comparing the $R_{O2,Pt}$ with the R_{O2} results in Figures 5 and 6 shows that the increase in resistances occurs at a much lower Co level for $R_{O2,Pt}$. To understand this, one must recognize the differences between the two cases. (1) limiting current test requires passing current through the MEA, thus causing Co to migrate and concentrate in the cathode (4, 12, 13). The true Co concentration in the cathode during test, therefore, is higher than the nominal level. (2) ionomer in the electrode is very thin (<10 nm) and is in contact with either Pt or carbon, while in the membrane it is much thicker (>10 μm). Thinner ionomer films have a less-developed hydrophilic-hydrophobic segregated structure due to the confinement effect, thus is more prone to cation effect. [ref Ahmed cation-doped GIXAS].

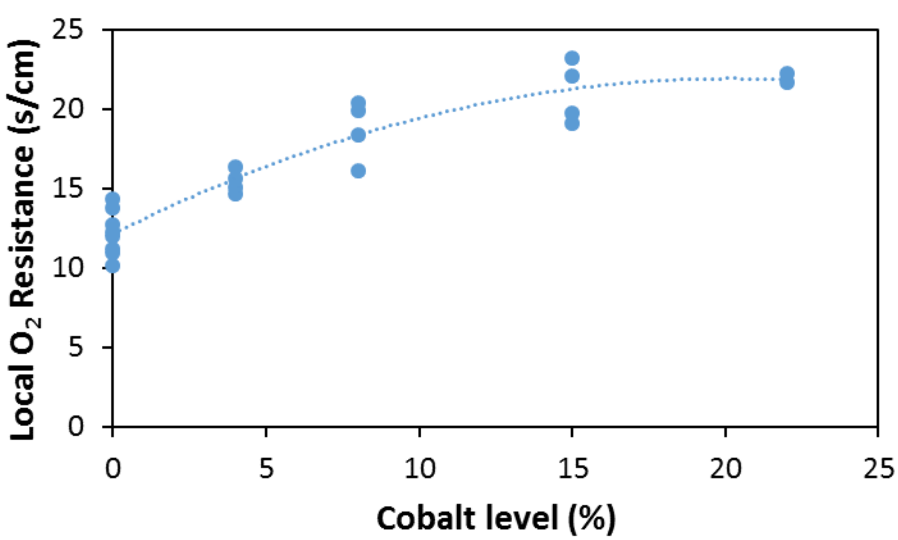

Figure 9. Local O2 resistance of a Pt/Vulcan cathode as a function of Co^{2+} exchange in the membrane. The resistances were determined at 80°C, 62% RH. The MEA was fabricated with 18 μm thick PFSA membrane, 0.05 mg_{Pt}/cm^2 Pt/Vulcan cathode with 0.8 ionomer/carbon ratio.

In a state-of-the-art fuel cell MEA, with Pt_3Co cathode (0.1 mg_{Pt}/cm^2_{MEA}) and 14 μm thick membrane, the Co exchange is expected to be in the range of 3 to 10% throughout its life [ref AMR 2017 and DOE status]. As current is applied, electric field gradient can cause migration of cations to the cathode, while redistribution of water throughout the MEA can also cause cation concentration to be nonuniform locally. These impact not only gas permeability, but also proton conduction and ORR activity. As shown in this work, the impact can be minimal under low current densities and extreme under high current densities.

Our results for each of these cases demonstrate the impact of this range of contamination levels on the ability of the PFSA films to allow oxygen delivery to the catalyst surface.

Conclusions

In this work, we successfully characterized the effects of monovalent (Li and Na) and divalent (Ni and Co) cations on the oxygen transport properties of bulk membrane and showed a negligible effect due to trivalent Ce at the low contamination levels consistent with its addition to the membrane for radical scavenging purposes (14, 15). We found that for full exchanges of these cations (Li, Na, Ni, Co), the increase in the R_{O2} at low water content was at least 100% and was less than 50% at a very high water content. At intermediate Co loadings, we found R_{O2}

plateaus for both high and low Co concentrations in the ionomer, leading to the hypothesis that a critical concentration exists where the membrane's hydrophilic domains become more tortuous, corresponding to an increase in the R_{O2}.

Based on the data collected for the mono- and divalent cations, we were able to form hypotheses on each possible hydrophilic domain deformation mechanisms' contribution to the R_{O2}. Our results indicated that contaminant cations reduce the oxygen permeability (increase the R_{O2}) in 3 ways: forming stronger ion pairs, reducing water uptake (except Li), and forming ionic cross-links (for multivalent cations). We hypothesize that these mechanisms affect oxygen transport by compressing the hydrophilic domain and increasing the tortuosity of the oxygen diffusion path. We found that these effects were strongly impacted by the hydration state of the membrane, due to water's ability to shield the electrostatic interactions between the cations and the sulfonate groups. Thus, the hydrophilic domain compression and tortuosity effects for contaminated membranes at higher hydration states is likely suppressed, leading to a smaller increase in the R_{O2}.

The results of this work will help inform the design process of PEMFCs as well as their operating conditions. PEMFC designers would do well to minimize the number of contaminant cations in the ionomer, to prevent full exchanges at the catalyst surfaces under high current densities, and to ensure that the fuel cells are hydrated to at least a medium level (60% RH or greater) in order that the effects of any contaminant cations are minimized. In addition, these results provide design insights for future ionomers with less susceptibility to increased R_{O2} with cation contamination. With the knowledge of the effects of these contaminant cations on oxygen transport, we hope that they can be accounted for, allowing for a further reduction of the catalyst loading and ultimately mass-market penetration by PEMFC technology.

Acknowledgments

This work was partially supported by the U.S. Department of Energy, Office of Energy Efficiency and Renewable Energy under grant DE-EE0007271.

A special thank you to Dr. Md. Aman Uddin, Leiming Hu, and Shohei Ogawa for their general assistance in the lab towards the completion of this work and their editorial contributions towards this publication.

References

1. U. S. DOE, *DOE Hydrogen and Fuel Cells Program Record* (2015).
2. A. Kongkanand and M. F. Mathias, *J Phys Chem Lett*, **7**, 1127 (2016).
3. H. Liu, W. K. Epting and S. Litster, *Langmuir*, **31**, 9853 (2015).
4. T. Greszler, T. Moylan and H. Gasteiger, *Handbook of Fuel Cells* (2009).
5. Y. Cai, A. Kongkanand, W. Gu and T. E. Moylan, *ECS Transactions*, **69**, 1047 (2015).
6. T. Okada, Y. Ayato, M. Yuasa and I. Sekine, *The Journal of Physical Chemistry B*, **103**, 3315 (1999).
7. T. Okada, J. Dale, Y. Ayato, O. A. Asbjørnsen, M. Yuasa and I. Sekine, *Langmuir*, **15**, 8490 (1999).
8. T. Okada, S. Møller-Holst, O. Gorseth and S. Kjelstrup, *J. Electroanal. Chem.*, **442**, 137 (1998).
9. H. A. Gasteiger, S. S. Kocha, B. Sompalli and F. T. Wagner, *Applied Catalysis B: Environmental*, **56**, 9 (2005).
10. F. D. Coms, H. Liu and J. E. Owejan, *ECS Transactions*, **16**, 1735 (2008).
11. H. R. Colón-Mercado and B. N. Popov, *J. Power Sources*, **155**, 253 (2006).
12. A. Z. Weber and C. Delacourt, *Fuel Cells*, **8**, 459 (2008).
13. B. L. Kienitz, H. Baskaran and T. A. Zawodzinski, *Electrochim. Acta*, **54**, 1671 (2009).
14. A. M. Baker, J. H. Dumont, R. Mukundan, S. G. Advani, A. K. Prasad, D. Spernjak and R. L. Borup, *ECS Transactions*, **80**, 643 (2017).
15. A. M. Baker, D. Torraco, E. J. Judge, D. Spernjak, R. Mukundan, R. L. Borup, S. G. Advani and A. K. Prasad, *ECS Transactions*, **69**, 1009 (2015).
16. S. Shi, A. Z. Weber and A. Kusoglu, *Electrochim. Acta*, **220**, 517 (2016).
17. K. Broka and P. Ekdunge, *J. Appl. Electrochem.*, **27**, 117 (1997).
18. M. Schalenbach, T. Hoefner, P. Paciok, M. Carmo, W. Lueke and D. Stolten, *The Journal of Physical Chemistry C*, **119**, 25145 (2015).
19. M. Schalenbach, M. A. Hoeh, J. T. Gostick, W. Lueke and D. Stolten, *The Journal of Physical Chemistry C*, **119**, 25156 (2015).
20. R. Jinnouchi, K. Kudo, N. Kitano and Y. Morimoto, *Electrochim. Acta*, **188**, 767 (2016).
21. K. A. Page, A. Kusoglu, C. M. Stafford, S. Kim, R. J. Kline and A. Z. Weber, *Nano Lett.*, **14**, 2299 (2014).